



Abnormal noise identification of engines based on wavelet packet transform and bispectrum analysis

Xingguo Yang^{1,2} , Ya Zhang² and Xujun Li^{1,3}

Abstract

Abnormal noise is the most prominent problem for motorcycles and affects the consumers' purchasing desire and driving experience and the enterprise's competitiveness. Usually, the noise from a newly assembled engine is detected by manual auscultation (MA) to determine if the engine is operating normally. However, MA is also affected by subjective and objective factors with severe labor intensity, and its accuracy greatly fluctuates. Importantly, MA cannot be applied in a corporation with mass production and high-quality requirements. To improve the efficiency and accuracy of motorcycle engine quality inspection and achieve intelligent production, an online engine abnormal noise detection method was proposed based on wavelet packet transform (WPT) and bispectrum analysis (BA); this method improved the accuracy and stability of the identification of the abnormal noise engine and reduced the cost of the check. First, the acoustic signal of the engine of the motorcycle was acquired by using a free-field microphone. Second, the background noise of signals was eliminated by using the wavelet correlation coefficient (WCC) theory, and the signal features were extracted by applying WPT and BA. Third, the feature vectors were normalized before being used as support vector machine (SVM) samples. Fourth, an appropriate kernel function and parameters were selected to train the vector machine using the training sets. Finally, the testing sets were used to inspect the accuracy of the vector machines. The result showed that the training accuracy is 95% and the testing accuracy is 97.5% of the samples were suitable by using the method of wavelet packet transform-bispectrum analysis-support vector machines (WPT-BA-SVM). WPT-BA-SVM effectively identified engine fault types and provided the theoretical foundation for the establishment of an engine abnormal noise online detection system.

Keywords

Abnormal noise, wavelet correlation coefficient, wavelet packet transform, bispectrum analysis, support vector machines

Date received: 27 October 2023; accepted: 14 December 2023

Handling Editor: Chenhui Liang

Introduction

In addition to the power, fuel economy, and safety of the vehicle, the noise, vibration, and harshness (NVH) performance of the vehicle has recently received much attention from consumers and enthusiasts. The clear engine working sound, the thick closing-door sound, and the crisp gearshift sound affect consumers and enhance their purchase desire and driving experience. Almost all car companies have established NVH departments to improve the comfort performance of

¹School of Automotive Engineering, Wuhan University of Technology, Wuhan, China

²School of Intelligent Manufacturing and Automotive Engineering, Chongqing Technology and Business Institute, Chongqing, China

³SINOTRUK Liuzhou Yunli Kodiak Machinery Co., Ltd., Liuzhou, China

Corresponding author:

Xingguo Yang, School of Intelligent Manufacturing and Automotive Engineering, Chongqing Technology and Business Institute, No. 15 Siyuan Road, University Park, Hechuan District, Chongqing 401520, China.
 Email: yanglixgy@163.com



Creative Commons CC BY: This article is distributed under the terms of the Creative Commons Attribution 4.0 License (<https://creativecommons.org/licenses/by/4.0/>) which permits any use, reproduction and distribution of the work without further permission provided the original work is attributed as specified on the SAGE and Open Access pages

(<https://us.sagepub.com/en-us/nam/open-access-at-sage>).

the entire car. However, in the process of manufacturing and using vehicles, the problem of abnormal noise is inevitable. Preventing cars with abnormal noise from entering the market and solving abnormal noise problems in a timely manner is an effective way for car enterprises to enhance brand competitiveness.

Vehicle abnormal noise is mainly divided into engine abnormal noise, chassis abnormal noise, and body abnormal noise. Of these, engine abnormal noise accounts for the highest proportion and is also the most difficult to control and solve. Engine abnormal noise with a wide frequency distribution comes from many different noise sources, such as combustion noise and mechanical noise.

Engine abnormal noise identification is generally divided into four steps: signal acquisition, signal filtering, feature extraction, and fault identification. In the process of signal acquisition, the environmental noise inevitably has been mixed into the engine signal, which needs to be appropriately removed to restore the true signal. Short-time Fourier transforms (SFTs) and wavelet transforms (WTs) are two common denoising methods. Notably, WT not only retains many advantages of SFT but can also process the signal more finely in the time-frequency domain and can better reflect certain mutation features of the signal. WT satisfies the requirement of localized and multiscale analysis of the signal in the time-frequency domain; thus, it is more widely used in the signal analysis field. The accuracy of signal characteristics is very important because it directly affects the result of the later type identification of abnormal noise and the progress of the study of the failure mechanism. Many methods have been applied to the feature extraction of signals, such as wavelet transform (WT),^{1–3} wavelet packet transform (WPT),⁴ empirical mode decomposition (EMD),^{5–10} local mean decomposition (LMD),^{11–15} ensemble empirical mode decomposition (EEMD),¹⁶ and bispectrum analysis (BA).^{17–21}

A satisfactory effect occurs when EMD is applied to address the nonlinear and nonstationary signals, which can decompose complex signals into several intrinsic mode functions (IMFs). However, the EMD algorithm has some problems, such as modal aliasing, nonunique decomposition results, and severe influence from Gaussian noise. To overcome the drawbacks of EMD, its combination with other algorithms is an effective approach. Bi et al. combined WT and EMD to extract gasoline engine vibration knock signals,⁷ and Li et al. combined ranging angle technology and EMD to extract the characteristics of diesel engine vibration signals.⁶ Compared to traditional EMD, EEMD can avoid the problem of modal confusion in the modal decomposition. Wu et al. proposed a new EEMD, which utilized the full advantage of the statistical characteristics of white noise to perturb the signal in its true

solution neighborhood and to improve the EMD algorithm.¹⁶ However, EEMD still could not completely solve the problem of modal aliasing of EMD. In addition, LMD decomposed the signal into a local mean and detail parts, avoiding the modal aliasing problem of EMD, and the decomposition results were more reliable. Zhao et al. proposed a compound interpolation envelope LMD through a novel envelope construction method and applied it to the fault diagnosis of compressor bearings.¹⁴ However, the LMD method required long-term decomposition of the signal, which was prone to signal drift, frequency aliasing, and other issues during the long-term calculation process.

The continuous wavelet algorithm was applied to the fault signal diagnosis of internal combustion engines and their cooling systems by Wu et al. and achieved good results.¹ To extract more detailed signal information, they applied WPT technology to extract acoustic signal features and combined it with artificial neural networks to establish a fault diagnosis system for internal combustion engines.⁴ Jiang et al. proposed a fault diagnosis method for electric vehicle power lithium batteries based on wavelet packet decomposition.²² Compared to traditional power spectrum analysis or autocorrelation function analysis, BA had better nonlinear analysis ability and could detect the nonlinear characteristics and secondary phase coupling frequency of signals. Zhou et al. applied a horizontal slice of cyclic bispectrum in rolling element bearings fault diagnosis and obtained a relatively good effect.²³

Statistical learning theory (SLT), a breakthrough result of statistical inference theory research, laid the foundation for the establishment of modern statistical learning theory, Vapnik–Chervonenkis (VC) theory; this theory not only satisfactorily answered the theoretical questions arising in artificial neural networks on a strict mathematical basis but also derived a new learning method, support vector machine (SVM). Aiswarya et al.²⁴ proposed an adaptive scheme that is based on a two-level SVM classifier model accurately detects the volatile changes in the microgrid under normal and fault conditions. This method has high accuracy and computational speed in fault identification.

Engine abnormal noise can be classified into mechanical noise, combustion noise, and intake/exhaust noise. Among them, mechanical noise caused by gears,^{25–27} bearings,^{28–31} and crankshafts^{32–33} accounts for the largest proportion. Diagnosing and monitoring mechanical system faults is crucial for resolving and preventing engine abnormal noise. Vibration analysis is one of the mainstream tools for studying faults in rotating machinery. The vibration signal characteristics of gears are influenced by the degree of gear wear and its features. Similarity-based methods for characterizing gear wear states can aid in vibration signal feature extraction and gear health

management. Feng et al.²⁵ proposed a new approach based on transmission error indicators to assess fatigue severity and predict the remaining lifespan of a gearbox by studying the relationship between gear wear/fatigue and transmission error signal characteristics and achieved promising results. Engine abnormal noise falls under the category of complex faults, where machine learning and deep learning are commonly applied in composite fault diagnosis and detection.

Although WT, WPT, and BA have been widely applied in the field of fault diagnosis, most of their research objects have been gasoline engines, diesel engines, and mechanical components such as gears and bearings, and there are few motorcycle engines used as research objects. In addition, vibration analysis techniques are the mainstream methods for mechanical fault diagnosis, and few articles focus on studying engine sound signals as research subjects. An abnormal noise detection approach is proposed based on WPT and BA for motorcycle engines, intending to improve the efficiency and accuracy of abnormal engine noise detection in enterprises while reducing labor intensity.

A total of 160 motorcycle engines were selected through manual auscultation as test samples, with four different types of engines accounting for 25% each. The engine sound signal was obtained through near-field detection, the noise components in the signal were removed using WCC technology, the signal features were extracted using WPT and BA technology, and the normalized signal features were randomly divided into training sets and testing sets as input vectors for SVM. The kernel function and parameters of the SVM were determined by empirical and grid search (GS) methods, respectively. The GS-SVM classifier was trained and tested through the feature database. The training and testing results showed that the classifier had appropriate accuracy and performance. This abnormal noise detection method based on WPT-BA-SVM technology provided an important technology for achieving the online detection of motorcycle engine abnormal noise.

Experimental method

Experimental conditions

The 110cc single-cylinder four-stroke motorcycle engine was selected as the object of the study, and the technical parameters of the engine are listed in Table 1. According to self-check and market feedback, mechanical abnormal noise was the major form of engine abnormal noise. For statistical convenience, engine abnormal noise types were divided into several types according to the sound source or characteristics of the signal by the manual auscultation (MA) method, such as crankcase abnormal noise, right cover abnormal noise, and squeal abnormal noise. The proportion of

Table 1. The main technical parameters of the engine.

Cylinder working volume	102 ml
Compression ratio	9:1
Rated power (kW)	4.95
Maximum power (kW)	6.2
Maximum torque (N.m)	7.07
Ignition mode	GDI
Start-up method	Motor/Backlash
Cooling media	Wind
Number of gears	4
Transmission ratio (1-4)	3.167, 1.941, 1.381, 1.095

Table 2. The proportion of the type of abnormal noise engine.

Types	Proportion	Types	Proportion
crankcase	56%	cylinder head	1%
right-cover	17%	others	12%
Squeaking	10%	total	100%
Left-cover	4%		

each abnormal noise type is provided in Table 2. In this paper, the three types of abnormal noise with the highest proportions were selected for testing and research.

Signal acquisition

The experimental system for acquiring acoustic signals from engines is shown in Figure 1. The engine was driven by a conveyor belt into the inspection window in turn, its position was detected by a sensor (not drawn in Figure 1), and the position signal was transmitted to the computer via signal collector 2. When the computer detected that the engine was in the correct inspection position, the quality inspector started the engine. The engine speed was monitored by sensor 1 and transmitted to the computer through collector 1. Sensor 2 began to collect signals when the engine idle speed stabilized and transmitted the signals to the computer via collector 1. LABVIEW was used to design the signal acquisition program, while MATLAB was used to implement the signal analysis function. This human-machine combination method used to detect engine abnormal noise has high automation and intelligence, which shortens the detection cycle, improves detection accuracy, and realizes the assembly line operation of engine noise detection. The specific signal acquisition and data analysis process is shown in Figures 2. Sensor 2 was a free-field microphone, the model number is MPA201, and its main technical parameters are listed in Table 3. Signal Collector 1 and Signal Collector 2 were both NI-USB9234 kits, and their main technical parameters are provided in Table 4.

The signal of an engine is greatly affected by its working conditions, such as its temperature, speed, and

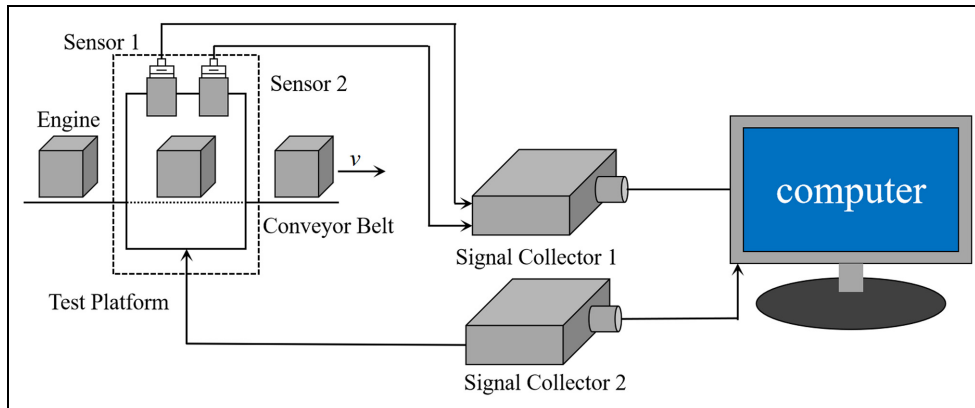


Figure 1. Schematic diagram of the engine noise test platform.

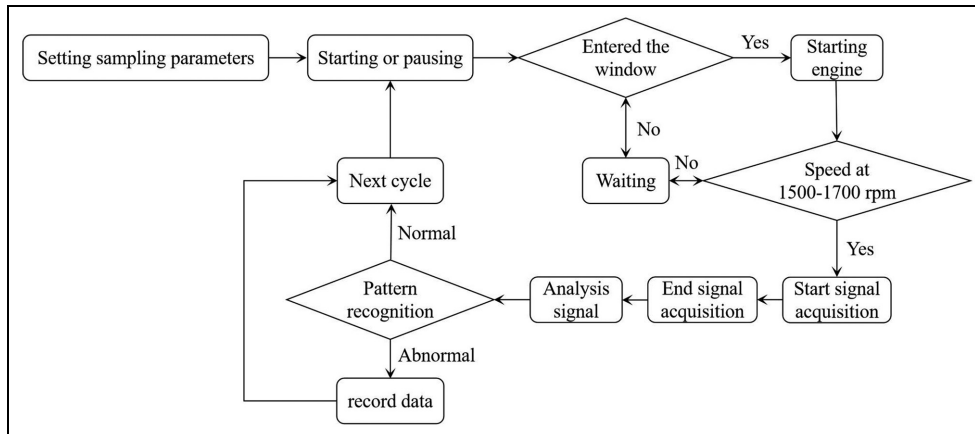


Figure 2. Flow chart of signal acquisition and data analysis.

Table 3. The parameters of the MPA201 microphone.

Sensitivity	45.7 mV/Pa	Output resistance	<50Ω
Frequency range	20~20 kHz	Humidity	0~95%
Dynamic range	16~134 db	Output Interface	BNC
Background noise	<16 db		

load. Therefore, the working condition of an engine needs to be determined before signal acquisition. Based on experience, the working conditions for abnormal noise identification of engines were set as follows: the

engine speed was 1500 to 1700 rpm and is monitored by sensor 2 in Figure 2, the engine load was idling, and no preheating was considered.

The mechanical noise of the engine originated from the vibration of the parts subject to external force, and the vibration energy was radiated outwards through the shell to form a sound signal. To obtain a signal with a high signal-to-noise ratio, the measurement point needed to be set on the path of maximum radiation energy. In this paper, the sound intensity method and the interactive filtering technique were used to determine the sensor installation location, and the mounting position of sensor 2 is shown in Figure 3. The distance

Table 4. The technical parameters of UI-USB9234.

Number of channels	4	Excitation current (mA)	2
Resolution(bit)	24	Dynamic range (dB)	102
Sampling rate(ks/s)	51.2	Input Resistance (k Ω)	305
Voltage Range(V)	-5~5	Interface	BNC
Operating temperature(°C)	-40~70	Size (mm)	130 × 90 × 33

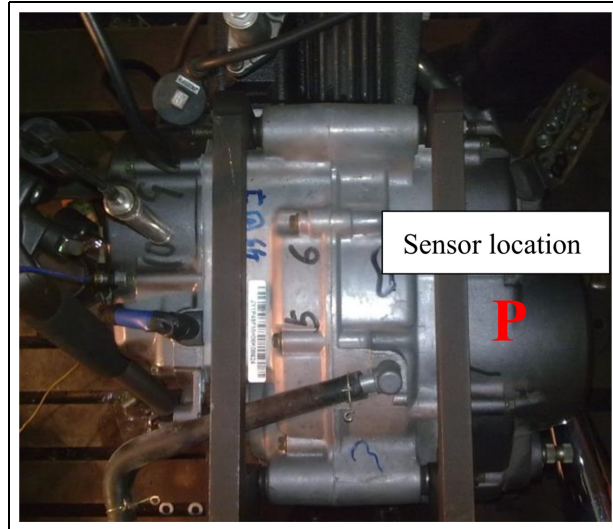


Figure 3. Location of sensor 2 in the test platform.

between the sensor and the engine case surface was 20 cm. In addition, the sampling frequency was 20,480 Hz, and the sampling time was 2 s.

Methodology

Wavelet coefficient correlation filtering

The engine acoustic signal collected from the workshop contains strong background noise; thus, a suitable method of denoising is required to restore the real signal. Compared with common signal denoising methods, such as independent component analysis, empirical mode decomposition, and blind source separation, wavelet denoising has good temporal and frequency localization performance, highlights the signal features, and weakens the noise characteristics; therefore, it is one of the most widely used analysis methods in the field of mechanical fault diagnosis. After more than 40 years of development, wavelet analysis has produced different noise reduction theories and noise reduction methods. To date, three wavelet noise reduction methods have been widely used: the mode maxima method,³⁴ the wavelet threshold method,³⁴ and the wavelet correlation coefficient method (WCC).³⁶ In this paper, the wavelet correlation filtering method was used to remove the background noise of the engine sound signal. Compared with the mode maxima method and threshold method, WCC had stable filtering performance, a high signal-to-noise ratio, a small mean square error, and high smoothness after filtering and could restore the real signal more accurately.

The results of the wavelet transform of signal and noise had significantly different correlations. The wavelet coefficients of the signal showed an evident correlation between scales, especially in the vicinity of the

mutation or edge, and the correlation coefficient between layers also became larger with increasing decomposition scale. Noise did not have this property, its energy was mostly concentrated at small scales, and the correlation coefficient generally did not change with increasing decomposition scale. A comparison of the magnitude of the correlation coefficients and wavelet coefficients can effectively be used to determine whether the wavelet coefficients are caused by signal or noise. After performing relevant calculations on wavelet coefficients, the wavelet coefficients generated by noise are weakened or eliminated, while those generated by the signal are retained or enhanced. Reconstructed wavelet coefficients were used to restore the real signal through inverse wavelet transform.

If the wavelet coefficients are generated by the signal, the correlation coefficients increase; if the wavelet coefficients are generated by the noise, the correlation coefficients decrease. These characteristics are used to determine whether the wavelet coefficients at that point should be retained or discarded.

The wavelet correlation coefficient is defined as follows:

$$Coor_j(k, n) = \prod_{i=0}^{j-1} W_f(k+i, n) \quad (1)$$

where $W_f(k, n)$ is the wavelet transform coefficient at scale k and position n and j is the number of scales of related operations; generally, $j = 2$, the correlation coefficients between two adjacent scales need to be calculated, and the correlation coefficient at this point is defined as follows:

$$Coor_2(k, n) = W_f(k, n) \times W_f(k+1, n) \quad (2)$$

Normalization needs to be performed to cause a uniform magnitude of correlation coefficients and wavelet coefficients, and it is always defined as follows:

$$NorCoor_2(k, n) = Coor_2(k, n) \sqrt{\frac{Pw(k)}{P_{Coor_2}(k)}}, n = 1, 2, \dots N \quad (3)$$

$$Pw(k) = \sum_{n=1}^{N} W_f(k, n)^2 \quad (4)$$

$$P_{Coor_2}(k) = \sum_{n=1}^{N} Coor_2(k, n)^2 \quad (5)$$

where N is the length of the time sequence.

The WCC filtering method can remove background noise by using the different correlations between the signal and noise, and the general process is shown in Figure 4. Calculating the normalized correlation

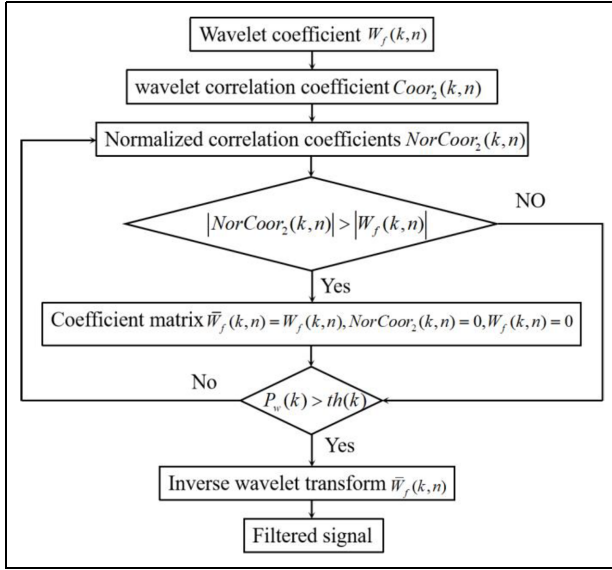


Figure 4. Flow chart of WCC filtering.

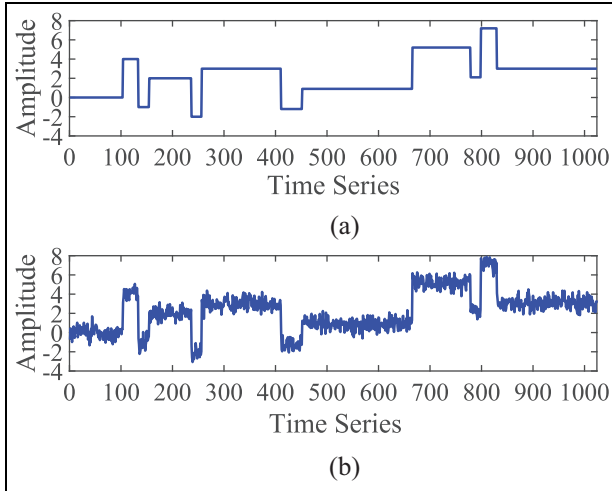


Figure 5. Results for analog signals: (a) original signal and (b) noised signal.

coefficient and comparing values of the correlation coefficients and wavelet coefficients are both iterative processes, and the termination conditions of the iterations are related to the threshold. Generally, the variance of noise energy on each scale is used as the threshold, and the accuracy is relatively high. Based on experience, in this paper, the variance of the wavelet coefficients of the first 80 data points of the signal is used as the noise energy threshold for each scale.

To verify the denoising effect of WCC filtering, the “Blocks” signal with 1024 data points was selected from the MATLAB signal library, and Gaussian white noise with a signal-to-noise ratio of 5 was added. The details of the simulated signals are shown in Figure 5. The

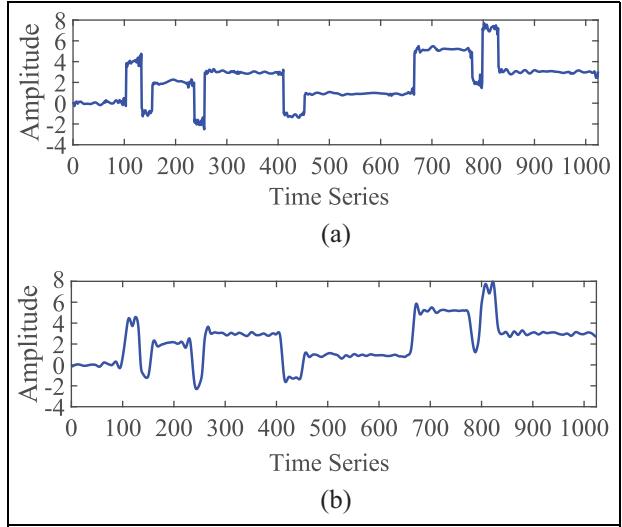


Figure 6. Comparison of the filtering results. (a) WCC filtering and (b) threshold method.

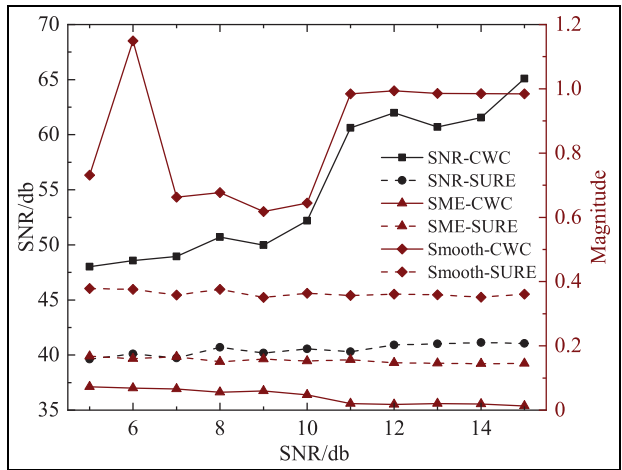


Figure 7. Comparison of the filtering effect of WCC and SURE.

simulation signals with Gaussian noise had many burrs, and specific information was difficult to identify. The WWC filtering and the threshold method were used for noise reduction, and the results of denoising are shown in Figure 6.

Both methods could restore most of the information of the original signal; however, the signal boundary after wavelet correlation filtering was more distinct, the horizontal segment was smoother, the burr was less, and the filtering effect was even better. To evaluate the two filtering methods more objectively, three indicators of signal-to-noise ratio (SNR), mean square error (SME), and smoothness to evaluate their filtering effects in multiple dimensions were used, and the results are shown in Figure 7. All three evaluation indicators of wavelet correlation filtering were better than those

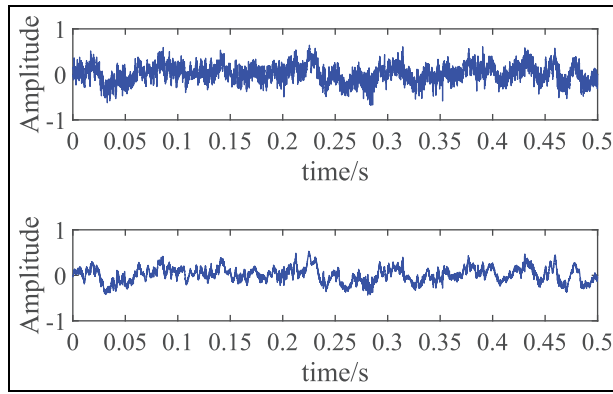


Figure 8. Time-domain signals of the engine (a) before filtering and (b) after filtering.

of the threshold method. Therefore, WCC filtering can be used for engine noise reduction processing. Figure 8 shows the result of the WCC filtering of the engine acoustic signal; the noise component was controlled within an acceptable range.

Wavelet packet transform theory

The one-dimensional time-domain signal f was projected onto the two-dimensional “time-scale” space through wavelet transform and decomposed throughout the entire analysis frequency domain. First, the signal was divided into two parts: high-frequency A1 and low-frequency D1 in the full frequency domain, and then low-frequency A1 was decomposed into high-frequency A2 and low-frequency D2 again; this approach was followed to decompose all frequency domains. Notably, the wavelet transforms only subdivided the low-frequency part of the signal and discarded the information of the high-frequency part of the signal. Unlike wavelet transform, wavelet packet transforms not only subdivided the low-frequency components of the signal but also decomposed the high-frequency information of the signal. Therefore, the wavelet packet transform had a higher frequency resolution.

We set $g_j^n(t) \in U_j^n$; then, $g_j^n(t)$ could be represented as follows:

$$g_j^n(t) = \sum_l d_l^{j,n} u_n(2^j t - 1) \quad (6)$$

The wavelet packet algorithm is as follows:

$\{d_l^{j,2n}\}$ and $\{d_l^{j,2n+1}\}$ can be calculated from $\{d_l^{j+1,n}\}$.

$$\{d_l^{j,2n}\} = \sum_k a_{k-2l} d_k^{j+1,n} \quad (7)$$

$$\{d_l^{j,2n+1}\} = \sum_k b_{k-2l} d_k^{j+1,n} \quad (8)$$

where $d_k^{j+1,n}$ in equations (7) to (8) is the result of the wavelet packet decomposition of the last layer, $\{d_l^{j,2n}\}$ and $\{d_l^{j,2n+1}\}$ are the results of wavelet packet decomposition of the next layer, j is the decomposition scale, l is the position indicator, n is the frequency index, k is a variable, a_{k-2l} and b_{k-2l} are multiresolution filter coefficients,

f_s is the sampling rate of a time-domain signal, and the maximum analysis frequency of the signal is $\frac{f_s}{2}$ according to the Nyquist sampling law. If the signal was decomposed into j -layer wavelet packets, as shown in Figure 6, the analysis frequency was evenly divided into 2^j segments. The width of each frequency band was $\frac{f_s}{2 \times 2^j}$ Hz. According to the Parseval energy equation, the energy of a time-domain signal could be expressed as the integral of the square of its amplitude over the entire time domain, as follows:

$$\|f(t)\|^2 = \int_{-\infty}^{+\infty} |f(t)|^2 dt \quad (9)$$

Since the amplitude of the wavelet packet coefficients represents the similarity between the wavelet packet function and the signal, the wavelet packet coefficients have energy properties, and $f(t)$ in equation (9) can be replaced by the wavelet packet transform coefficients. The energy of the signal is expressed as follows:

$$\|f(t)\|^2 = \sum_{k=0}^{2^j-1} |C_{j,k}|^2 \quad (10)$$

where j is the number of wavelet packet decomposition layers, and k is the number of frequency bands.

The steps to extract the wavelet packet energy spectrum of the engine signal were as follows:

- (1) Appropriate wavelet packet functions and decomposition levels were selected.
- (2) The wavelet packet energy spectrum of the signal in each frequency band was calculated according to equation (11), and this energy was normalized according to equation (12).

$$E_{j,k} = \sum_n |C_{j,k,n}|^2 \quad (11)$$

$$E'_{j,k} = \frac{E_{j,k}}{\sum_{k=0}^{2^j-1} E_{j,k}} \quad (12)$$

where $C_{j,k,n}$ is the wavelet packet coefficient, j is the scale of wavelet packet decomposition, k is the frequency band, and n is the position coefficient.

- (3) The normalized wavelet packet energy spectrum of each frequency band was used to form a part of the engine feature vector. The feature vector is defined as follows:

$$\mathbf{E} = [E'_{j,1}, E'_{j,2}, \dots, E'_{j,2^j-1}] \quad (13)$$

Wavelet packet energy spectrum of the signals

According to the manufacturer's self-inspection and market feedback data, the top three types of engine noise with the highest proportion are right-cover abnormal noise, crankcase abnormal noise engine and squeal abnormal noise, and left-cover abnormal noise. Notably, the type of abnormal sound was initially determined using artificial auscultation. To verify the effectiveness of the research method in this article, we selected 30 engines from each of the three engines with the highest proportion of abnormal noise and normal engines as the experimental objects. These engines were labeled Type 1 to Type 4, corresponding to normal engines, crankcase abnormal noise engines, right-cover abnormal noise engines, and squeal abnormal noise engines. The engine sound signal was extracted using the method in Section 2.2, and the background noise was removed using the method in Section 3.1.

Common wavelet mother functions include haar, db, sym, mexh, and so on. Usually, the value of entropy is used to measure the distance between the signal and the wavelet basis. The smaller the entropy value, the smaller the difference between the signal and the mother wavelet, and the larger the wavelet coefficient during signal decomposition.³⁰ According to the method introduced in Section 3.2, through comparative analysis, db4 was used as a wavelet packet function, and the number of decomposition layers was determined to be 4, which achieved better results. The normalized wavelet packet energy spectrum results of the signal are shown in Figure 9. The wavelet packet energy of the four types of engines was mainly concentrated in the low-frequency band, and more than 95% of the energy of the normal engine was concentrated in the first frequency band. However, the abnormal noise engines also had a significant energy distribution in the mid- or high-frequency band, such as the high wavelet packet energy spectrum of the crankcase abnormal noise engine in the second–eighth frequency band. The right cover abnormal noise machine had a higher wavelet energy spectrum in the 2nd–4th and 13th frequency

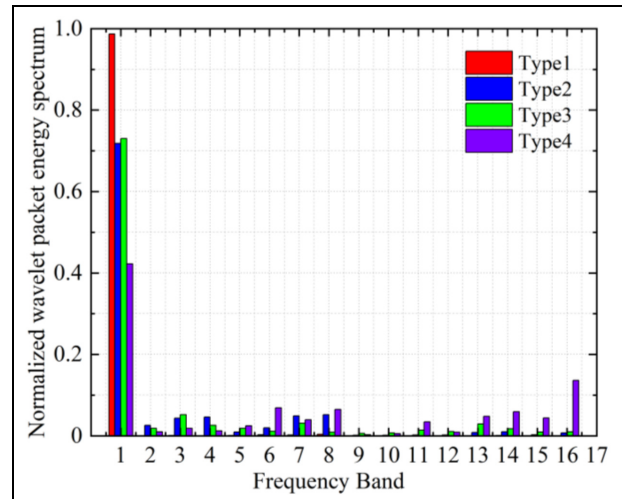


Figure 9. Wavelet packet energy spectrum distribution of the acoustic signals from the engine.

bands. The screamer had a significant wavelet packet energy distribution in the 6th–8th and 13th–16th frequency bands. The distribution of the wavelet packet energy spectrum varied among different types of engines; therefore, the wavelet packet energy spectrum of engine sound signals could be used as signal features.

Bispectrum analysis theory

The power spectrum describes the energy distribution of a time-domain signal in the frequency domain, and it is the Fourier transform of the autocorrelation function of the time-domain signal. Similar to the power spectrum solution process, the higher-order spectrum is a multidimensional Fourier transform of the higher-order accumulation of the signal and is widely used in engineering applications. Because the bispectrum has all the characteristics of the higher-order spectrum and is simple to solve, it is the most widely applied high-order spectrum.

x_n is a third-order smooth random time series with zero means, and its third-order cumulant is defined as follows:

$$C_{3,x} = E[x(n)x(n + \tau_1)x(n + \tau_2)] \quad (14)$$

The above equation satisfies the absolute summability condition:

$$\sum_{\tau_1}^{+\infty} \sum_{\tau_2}^{+\infty} |C_{3,x}(\tau_1, \tau_2)| < +\infty \quad (15)$$

The result of the two-dimensional Fourier transform of the third-order accumulation of equation (14) is as follows:

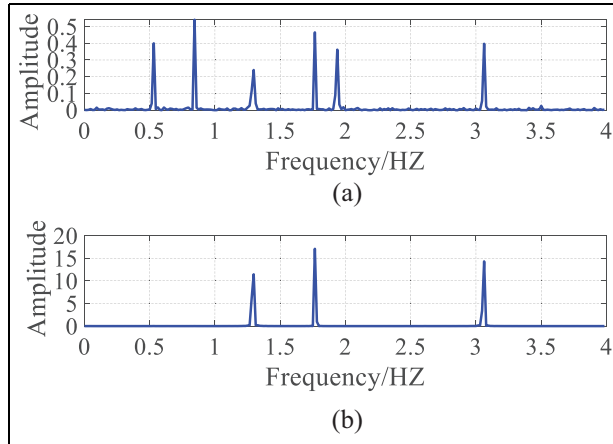


Figure 10. Analysis results of the simulation signals: (a) power spectrum and (b) bispectrum diagonal slicing.

$$B_{3,x}(w_1, w_2) = \sum_{\tau_1}^{+\infty} \sum_{\tau_2}^{+\infty} C_{3,x}(\tau_1, \tau_2) e^{-j(w_1\tau_1 + w_2\tau_2)} \quad (16)$$

Because bispectrum analysis has symmetry and to aid in the calculation, the relationship between τ_1 and τ_2 was set as $\tau_1 = \tau_2 = \tau$ and the diagonal slices of the third-order cumulants of the random time series could be acquired. Then, a one-dimensional Fourier transform was performed, and the $1\frac{1}{2}$ dimensional spectrum of this random time series could be obtained.

The simulation signal is composed of the following:

$$x(t) = \sum_{i=1}^6 \cos(2\pi f_i t + \varphi_i) + w(n) \quad (17)$$

where $w(n)$ is Gaussian white noise, which is used to simulate the background noise. equation (17) contains six frequency information: $f_1 = 0.5281$, $f_2 = 0.8456$, $f_3 = 1.9323$, $f_4 = 1.2909$, and $f_5 = 1.7671$, and they satisfy the relationship $f_6 = f_4 + f_5$. In addition, all of the phases ($\varphi_1, \varphi_2, \dots, \varphi_5$) are independent uniformly distributed phase parameters in $[0 \sim 2\pi]$, and they satisfy the following equation: $\varphi_6 = \varphi_4 + \varphi_5$. A set of secondary phase coupling frequencies can be observed in equation (17). The power spectrum of the simulation signal is shown in Figure 10(a) and contains all frequency components of the signal; notably the energy of the simulation signal was also distributed at other frequencies. However, as shown in Figure 10(b), the peak energy of bispectrum diagonal slices of the simulation signal only appeared at f_4, f_5 , and f_6 , and there was no peak energy at f_1, f_2 , and f_3 . This indicated that secondary phase coupling frequencies of the signal could be detected by bispectrum analysis. In addition, the noise energy was greatly reduced through bispectrum analysis, which was a characteristic that the power spectrum did not have. Generally, a nonlinear signal deviating from the

Gaussian process occurs when mechanical equipment is abnormal, and the nonlinear relationship is expressed as the sum frequency or the difference frequency and sometimes as the integral multiple frequencies of the fundamental frequency. As shown in Figure 10, these frequencies with nonlinear relationships could be extracted by bispectrum analysis and used as feature vectors for pattern recognition of the faults.

There are two common bispectrum estimation methods: parametric and nonparametric methods. AR, MA, ARMA, and other models are often used in parameter estimation. The parametric estimation has high computational accuracy, but the operation process is complex and large, and it is difficult to determine the model parameters. However, nonparametric estimation has a small operation, a relatively simple computational method, moderate computational accuracy, and better engineering applicability. At present, there are two main methods of nonparametric estimation: the indirect method and the direct method. The main calculation process of indirect bispectrum analysis was as follows: first, the segment and mean processing of the signal was performed, the third-order cumulant per segment was calculated, and finally, a two-dimensional Fourier transform of the third-order cumulant was performed to obtain the bispectrum estimation of the signal. The main calculation process of direct bispectrum analysis was as follows: first, the signal was evenly divided into several parts, then the Fourier transform per part was performed, and finally, the double correlation calculation was performed on the results of the Fourier transform to obtain the bispectrum. In this paper, the direct bispectrum estimation of the Hosa toolbox in MATLAB was used to extract the features of engine signals.

Bispectrum of the signals

According to the theory of bispectrum analysis, as long as the signal contains some secondary phase coupling frequencies, the peak of the bispectrum will appear at the corresponding frequencies. The bispectrum distribution of the denoised signal is shown in Figure 11. Two extreme value areas of the bispectrum were distributed in the normal engine, and the coordinates of the center frequency were (140,160) and (320,340). In addition, the bispectrum peak of the normal engine was also distributed around the area whose coordinate of the center frequency was (3140,280). Compared with the normal engine, the bispectrum distribution range of the crankcase abnormal noise engine was wider, and multiple bispectrum peak regions were distributed below 3000 Hz. The center frequencies of the three regions with the highest bispectrum were (900,860), (1760,1740), and (2560,900). In addition, the bispectrum peak of the crankcase abnormal noise engine was also significantly

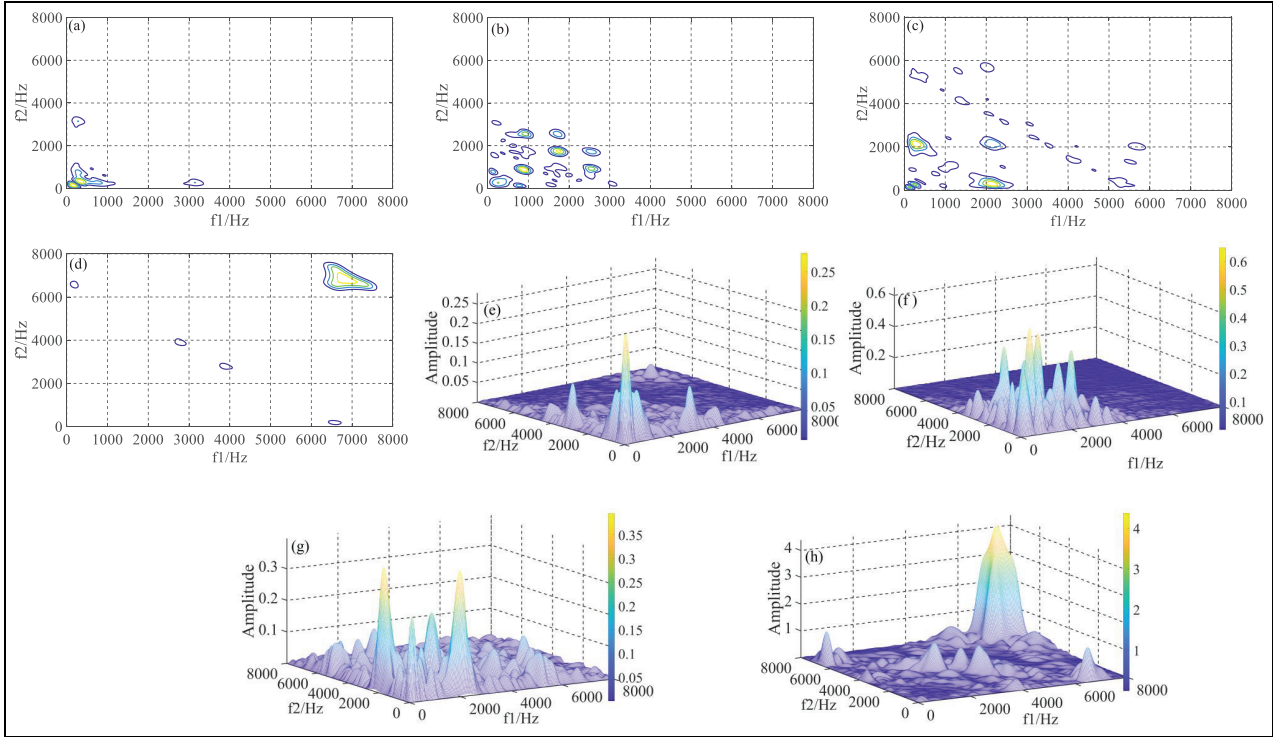


Fig. 11. Bispectrum distribution of the acoustic signals from engines (a)~(d) Contour plot of the bispectrum of Type I~Type 4. (e)~(h) Three-dimensional diagram of the bispectrum of Type I~Type 4.

higher than that of the normal engine. However, the maximum bispectrum value of the right-cover abnormal noise engine was similar to that of the normal engine and was lower than that of the other two classes of engines. The center frequencies of the two districts with the highest bispectrum were (2140,300) and (2200,2160). The apparent feature of the bispectrum distribution of the squeal abnormal noise engine was that the bispectrum values near the zone with center frequency (6860, 6820) were much higher than those in other zones, and the number of bispectrum peak regions was the least.

In Figure 11, the region of the secondary phase coupling frequency of the bispectrum varied with the engine type. Therefore, the features of engine signals could be collected through the result of bispectrum near the center frequency of secondary phase coupling, and the coordinates of the center frequencies assigned for bispectrum analysis were (140,160), (320,340), (900,860), (1760,1740), (2560,900), (2140,300), (2200,2160), and (6860,6820). Similar to the definition of the wavelet packet energy spectrum, the feature vector of bispectrum analysis of the engine signal is defined as follows:

$$B = [B'_1, B'_2, \dots, B'_8] \quad (18)$$

$$B'_i = \frac{B_i}{\sum_{i=1}^8 B_i} \quad (19)$$

$$B_i = \sum_{k_1=-100}^{100} \sum_{k_2=-100}^{100} |B_{3,x}(f_1 + k_1, f_2 + k_2)| \quad (20)$$

where (f_1, f_2) is one of the eight coordinates of the center frequency mentioned above and $B_{3,x}(f_1, f_2)$ is the result of bispectrum analysis of the engine signal.

Model training using WPT-BA-SVM and results

Sample preparation

Forty sample engines were selected using the MA method from the normal engine, the crankcase abnormal engine, the right-cover abnormal noise engine, and the squeal abnormal noise engine. In this way, the sample library consisted of 160 engines. The sound signal of each engine was obtained through the method in Section 2.2. First, the WCC filtering method was applied to remove the background noise of the signal, and WPT and BA were used to extract features of the signal that had been filtered. In summary, a total of 24 features were extracted from the engine sound signal, including 16 wavelet packet energy spectrum features and 8 bispectrum features. There were 160 sets of data features, and the partial data are shown in Table 5. The training set consisted of 120 samples randomly selected from the sample library, and the testing set was made up of the remaining samples.

Table 5. Engine signal features based on WPT and BA.

Number	Wavelet Packet energy spectrum(the first 6)						Bispectrum	Attribute	
	W	W ₁	W ₂	W ₃	W ₄	W ₅			
1	0.9866	0.0005	0.0009	0.0003	0.001	0.0028	0.3528	0.4115	0.1016
2	0.9850	0.0004	0.0008	0.0004	0.0013	0.0031	0.5967	0.2776	0.0178
3	0.9518	0.0006	0.0027	0.0011	0.0039	0.0116	0.4188	0.4323	0.0744
4	0.7183	0.026	0.0434	0.0464	0.0096	0.0198	0.0973	0.1635	0.2464
5	0.731	0.0592	0.0394	0.0386	0.0076	0.016	0.0535	0.3489	0.1383
6	0.7282	0.0376	0.0508	0.0362	0.0089	0.0189	0.0897	0.3225	0.1687
7	0.5648	0.0156	0.0502	0.0249	0.0566	0.0245	0.134	0.0833	0.0234
8	0.7802	0.0038	0.0305	0.0118	0.0197	0.012	0.157	0.1399	0.0758
9	0.5628	0.0103	0.0241	0.0211	0.0254	0.0314	0.0918	0.0772	0.0026
..
159	0.4224	0.01	0.0185	0.0122	0.0248	0.0686	0.019	0.026	0.0029
160	0.6027	0.0004	0.0076	0.0014	0.031	0.0391	0.0105	0.0355	0.0118

Model training and results

Support vector machine (SVM) evolved from statistical learning theory, which establishes a perfect and standard machine learning method based on statistical theory, avoids the arbitrariness of classification recognition scheme design, uses the principle of structural risk minimization to ensure the accuracy of the decision function and is a widely used pattern recognition method. Theoretical studies have shown that SVM can improve the computational speed and classification accuracy of vector machines if kernel functions are introduced for modeling and classification operations; thus, appropriate kernel functions need to be selected when support vector machines are used for pattern recognition. To improve the generalization ability of the RBF kernel function, two important parameters c and g of the kernel function can be determined by the appropriate method, and the sample data can be normalized to further improve the classification accuracy.

Recently, the popular methods for optimizing SVM kernel function parameters include grid search (GS), genetic algorithm (GA), and particle swarm optimization (PSO). Among them, the GA and PSO are heuristic algorithms whose calculation processes are quite complex. Additionally, the GA has a strong global search ability, but its local search ability is weak; PSO has a fast convergence speed but is prone to falling into local optima. Accordingly, an improved GS is used to optimize the parameters of the RBF kernel function.

The LIBSVM toolbox developed by Professor Lin's team at Taiwan University was used for model training and testing of the SVM. First, $C - SVC$ was selected as the classifier for SVM, and model accuracy was ensured by a 10-fold cross-validation (CV) method since it gives unbiased and reliable prediction results.³⁶ It is a standard practice to apply a 10-fold CV to the machine learning algorithm because it exhibits ideal prediction accuracy of compound faults in ball bearings.³¹ Then, the modified GS method was applied to optimize the kernel function parameters. The initial search scope for GS was $[2^{-8}, 2^8]$, the search step size was 2^3 , the preliminary training accuracy was 83.75%, and the approximate range of the optimal parameters was $[2^{-3}, 2^3]$. Therefore, the delicate search range for GS was $[2^{-3}, 2^3]$, the search step size was 2^{-3} , and the training accuracy was 95%. The optimal results of c and g were determined to be 0.125 and 0.25, respectively.

To verify the reasonableness of GS to determine the parameters of the kernel function, we also selected GA and PSO to calculate the parameters, and the results are shown in Figure 12 and Table 6. All three methods achieved relatively high model training accuracy, but the training accuracy of GS was slightly higher than that of the other two methods. In addition, GS had a shorter computation time with fewer iterations.

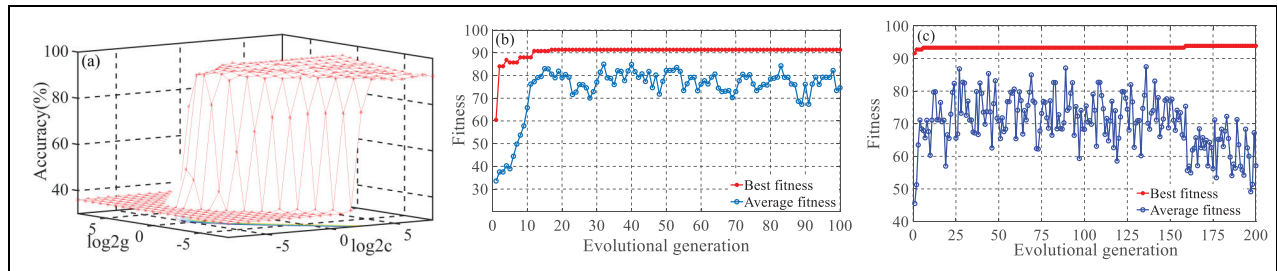


Figure 12. Results of the parameter optimization for the different methods: (a) grid search (GS), (b) genetic algorithm (GA), and (c) particle swarm optimization (PSO).

Table 6. Comparison of the results of the different parameter optimization methods.

Parameters	GS	GA	PSO
Range c	$[2^{-8}, 2^8]$		
Range g	$[2^{-8}, 2^8]$		
Best c	0.125	0.7233	5.0674
Best g	0.25	5.5694	2.2978
Accuracy (%)	95%	90.83%	93.33%
Time (s)	6.4	32.3	65.7

Table 7. Comparison of comprehensive performance of different detection methods.

Parameters	The method of MA	The method of this article
Average time (s)	50	12
Accuracy (%)	87	97.5
Cost of testing 400 engines (¥)	200	42
Stability of accuracy	Medium	Higher

Therefore, GS was a more appropriate method to compute the parameters of the kernel function.

A well-trained SVM was also used to identify abnormal noise types in the testing set. The test results are shown in Figure 13, and the testing accuracy was 97.5%. Practical experience showed that the identification accuracy could fluctuate as the number of samples increased. However, the recognition accuracy was predicted to remain above 90%. Therefore, our proposed WPT-BA-SVM had high accuracy in identifying abnormal noises and could be used for subsequent online detection processes of engine abnormal noise.

To further verify that the method proposed in this article can be used for online detection of engine noise, factors such as detection time, detection accuracy, and detection cost will be carefully considered. The specific results of the comparison are shown in Table 7. MA is a subjective evaluation method, and technicians often need to spend more time confirming abnormal noises.

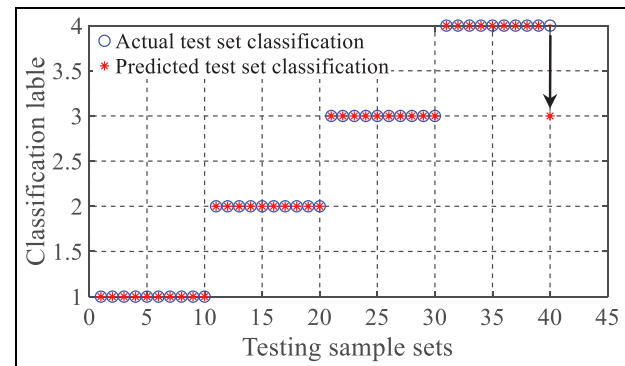


Figure 13. GS-SVM identification results of abnormal engine noise.

The average detection time is 50 s, which is nearly four times that of the method in this article. However, compared to MA, the method proposed in this article not only has a shorter detection cycle but also has higher and more stable accuracy, with a calculation time of about 8 s. In addition, the method used in this article adopts an automated engine transmission platform, reducing the engine logistics process of MA, making the process design more reasonable, and reducing detection costs by 76%. Therefore, the method proposed in this article can be used for online detection of engine noise.

Conclusions

To address the problems of unstable accuracy and severe labor intensity of MA for engine abnormal noise detection, an online engine abnormal noise detection scheme based on WPT and BA was proposed, which reduced labor intensity and simultaneously improved the accuracy and stability of abnormal noise detection. The conclusions of the study were as follows:

- (1) Our proposed WCC method was applied to filter noise because the wavelet coefficients of the

- signal and noise after the wavelet transform had different correlations, which could effectively remove the background noise of the signal and restore the real engine signal. The three indices of signal-to-noise ratio, mean square error, and smoothness were introduced to evaluate the denoising effect of WCC, and WCC was compared with the SURE denoising method. The results showed that the filtering effect of WCC was better than that of SURE and that WCC could be used for signal denoising.
- (2) Wavelet packet transform is widely used in mechanical fault diagnosis and pattern recognition, which reflects the distribution of signal energy in the time-frequency domain. The analysis frequency of the signal was evenly divided into 16 frequency bands, and the wavelet packet energy spectrum on each frequency band exhibited different characteristics. The distribution of the wavelet packet energy spectrum also greatly varied with different engine types. The secondary phase coupling frequency varied depending on the type of engine, which could be detected through bispectrum analysis, and bispectrum peaks in the zone were present near the secondary phase coupling frequency. Therefore, the features of the signal could be acquired using BA. The experimental results showed that the signal features extracted through WPT and BA had significant discrimination and could be used as input vectors for SVM.
- (3) The kernel function selection and parameter determination were the keys to improving the pattern recognition accuracy of the SVM. In this paper, the RBF kernel function was selected through experience, and the parameters c and g were determined through an improved GS. The testing accuracy of SVM reached 97.5%, which was a relatively satisfactory result even though it could decrease as the sample size increased. Therefore, our proposed WPT-BA-SVM was effective and could be applied in industry.
- (4) Although the method proposed in this article has a shorter detection time, higher accuracy, and satisfactory detection cost compared to MA, there are still some limitations that need improvement. For example, smaller sample sizes may lead to unstable detection accuracy, and other types of faults and compound faults, except for right-cover abnormal noise, crank-case abnormal noise engine and squeal abnormal noise, cannot be detected, full automation has not yet been achieved, and so on. To further enhance the efficiency and accuracy of

engine abnormal noise detection, a more intelligent online detection platform for engine abnormal noise needs to be researched. This platform will be capable of intelligent control of engine transmission, automatic engine start-stop, monitoring of engine position and rotation speed, and abnormal noise detection, among other key functions. Simultaneously, it is necessary to increase the sample size as much as possible and ensure the authenticity of the sample data to improve the credibility of the model detection results. Additionally, the recognition of other types of engine abnormal noise and compound faults will also be considered.

Declaration of conflicting interests

The author(s) declared no potential conflicts of interest with respect to the research, authorship, and/or publication of this article.

Funding

The author(s) disclosed receipt of the following financial support for the research, authorship, and/or publication of this article: This work was financed and fully supported by the Science and Technology Research Program of Chongqing Municipal Education Commission (Grant No. KJQN 202004005 and 202204015), which is greatly appreciated.

ORCID iD

Xingguo Yang  <https://orcid.org/0009-0003-5174-8000>

Data availability

The data of this study are available from the corresponding author upon request.

References

- Wu J and Chen J. Continuous wavelet transform technique for fault signal diagnosis of internal combustion engines. *NDT&E Int* 2006; 39: 304–311.
- Wu J and Liu C. Investigation of engine fault diagnosis using discrete wavelet transform and neural network. *Expert Syst Appl* 2008; 35: 1200–1213.
- Wu J and Liu C. An expert system for fault diagnosis in internal combustion engines using wavelet packet transform and neural network. *Expert Syst Appl* 2009; 36(3 Part 1): 4278–4286.
- Yan R, Gao R and Chen X. Wavelets for fault diagnosis of rotary machines: a review with applications. *Signal Process* 2014; 96(PartA): 1–15.
- Yao L, Zheng J, Xiao Y, et al. An intelligent fault diagnosis method for lithium-ion battery pack based on empirical mode decomposition and convolutional neural network. *J Energy Stor* 2023; 72(PartA): 108181.

6. Li Y, Tse P, Yang X, et al. EMD-based fault diagnosis for abnormal clearance between contacting components in a diesel engine. *Mech Syst Signal Proc* 2010; 24: 193–210.
7. Bi F, Ma T and Wang X. Development of a novel knock characteristic detection method for gasoline engines based on wavelet-denoising and EMD decomposition. *Mech Syst Signal Proc* 2019; 117: 517–536.
8. Nandi S and Reddy S. Understanding Failure analysis using harmonic analysis and empirical mode decomposition techniques. *Eng Failure Anal* 2022; 139: 106442.
9. Xue X, Zhou J, Xu Y, et al. An adaptively fast ensemble empirical mode decomposition method and its applications to rolling element bearing fault diagnosis. *Mech Syst Signal Proc* 2015; 62: 444–459.
10. Xia S, Zhang J, Ye S, et al. A mechanical fault detection strategy based on the doubly iterative empirical mode decomposition. *Appl Acoust* 2019; 155: 346–357.
11. Smith J. The local mean decomposition and its application to EEG perception data. *J R Soc Interf* 2005; 2: 443–454.
12. Zhang C, Li Z, Hu C, et al. (2017) An optimized ensemble local mean decomposition method for fault detection of mechanical components. *Meas Sci Technol* 2017; 28: 1–15.
13. Wang L, Liu Z, Miao Q, et al. Time-frequency analysis based on ensemble local mean decomposition and fast kurtogram for rotating machinery fault diagnosis. *Mech Syst Signal Proc* 2018; 103: 60–75.
14. Zhao H, Wang J, Lee J, et al. A compound interpolation envelope local mean decomposition and its application for fault diagnosis of reciprocating compressors. *Mech Syst Signal Proc* 2018; 110: 273–295.
15. Wang L, Liu Z, Miao Q, et al. Complete ensemble local mean decomposition with adaptive noise and its application to fault diagnosis for rolling bearings. *Mech Syst Signal Proc* 2018; 106: 24–39.
16. An X, Jiang D, Li S, et al. Application of the ensemble empirical mode decomposition and Hilbert transform to pedestal looseness study of direct-drive wind turbine. *Energy* 2011; 36: 5508–5520.
17. Guo J, Zhang H, Zhen D, et al. An enhanced modulation signal bispectrum analysis for bearing fault detection based on non-Gaussian noise suppression. *Measurement* 2020; 151: 107240.
18. Guo J, Zhen D, Li H, et al. Fault detection for planetary gearbox based on an enhanced average filter and modulation signal bispectrum analysis. *ISA Trans* 2020; 101: 408–420.
19. Mao Y, Jia M and Yan X. A new bearing weak fault diagnosis method based on improved singular spectrum decomposition and frequency-weighted energy slice bispectrum. *Measurement* 2020; 166: 108235.
20. Shen G, McLaughlin S, Xu Y, et al. Theoretical and experimental analysis of bispectrum of vibration signals for fault diagnosis of gears. *Mech Syst Signal Proc* 2014; 43(1–2): 76–89.
21. Gu F, Wang T, Alwodai A, et al. A new method of accurate broken rotor bar diagnosis based on modulation signal bispectrum analysis of motor current signals. *Mech Syst Signal Proc* 2015; 50: 400–413.
22. Jiang J, Zhang R, Wu Y, et al. A fault diagnosis method for electric vehicle power lithium battery based on wavelet packet decomposition. *J Energy Storage* 2022; 56(Part A): 105909.
23. Zhou Y, Chen J, Dong G, et al. Application of the horizontal slice of cyclic bispectrum in rolling element bearings diagnosis. *Mech Syst Signal Proc* 2012; 26: 229–243.
24. Aiswarya R, Nair DS, Rajeev T, et al. A novel SVM based adaptive scheme for accurate fault identification in microgrid. *Electr Power Syst Res* 2023; 221: 109439.
25. Feng K, Ji J and Ni Q. A novel gear fatigue monitoring indicator and its application to remaining useful life prediction for spur gear in intelligent manufacturing systems. *Int J Fatigue* 2022; 168: 107459.
26. Feng K, Ni Q, Beer M, et al. A novel similarity-based status characterization methodology for gear surface wear propagation monitoring. *Tribol Int* 2022; 174: 107765.
27. Feng K, Ji J, Ni Q, et al. A novel vibration-based prognostic scheme for gear health management in surface wear progression of the intelligent manufacturing system. *Wear* 2023; 522: 204697.
28. Tang G, Yi C, Liu L, et al. A novel transfer learning network with adaptive input length selection and lightweight structure for bearing fault diagnosis. *Eng Appl Artif Intell* 2023; 123(Part C): 106395.
29. Tang G, Liu L, Liu L, et al. Unsupervised transfer learning for intelligent health status identification of bearing in adaptive input length selection. *Eng Appl Artif Intell* 2023; 126(Part C): 107051.
30. Vakharia V, Gupta VK and Kankar PKA comparison of feature ranking techniques for fault diagnosis of ball bearing. *Soft Comput* 2015; 20: 1601–1619.
31. Suthar V, Vakharia V, Patel VK, et al. Detection of compound faults in ball bearings using multiscale-SinGAN, heat transfer search optimization, and extreme learning machine. *Machines* 2023; 11: 29.
32. Zhu S, Cong J, Yuan W, et al. Simulation of heavy-duty crankshaft sub-dynamics and experimental study of wear mechanisms. *Mater Today Commun* 2023; 36: 106826.
33. Wang Y, Luo Y, Mo Q, et al. Failure analysis and improvement of a 42CrMo crankshaft for a heavy-duty truck. *Eng Failure Analysis* 2023; 153: 107567.
34. Mallat S and Hwang W. Singularity detection and processing with wavelet. *IEEE Trans Inform Theory* 1992; 38: 617–643.
35. Donoho D. De-noising by soft-thresholding. *IEEE Trans Inform Theory* 1995; 41: 613–627.
36. Xu Y, Weaver J, Healy D, et al. Wavelet transform domain filter: a spatially selective noise filtration technique. *IEEE Trans Image Proc* 1994; 3: 747–758.